kcal/mol, somewhat lower than the TMM value but not greatly so. On the basis of the comparisons with more accurate wave functions in the TMM case, a crude estimate of the accuracy of our calculated excitation energies is ±3 kcal/mol. In addition, the variation principle for total energies (Table IV) provides a rough guide for comparisons with other calculations.

The pattern of substituent effects on the TMM excitation energies is found to be reasonably consistent with models for alkyl stabilization of radical centers.

**Acknowledgment.** We are grateful for helpful conversations with J. A. Berson, W. T. Borden, E. R. Davidson, D. A. Dixon, and H. F. Schaefer. Computer time was provided by the Ohio State Instruction and Research Computer Center.

**Registry No.** I, 60743-11-5; II, 32553-01-8; trimethylenemethane, 13001-05-3.

# Probing of Chemical Bonding through Two-Photon Spectroscopy of Substituted Benzenes

**Richard P. Rava and Lionel Goodman***

*Contribution from the Department of Chemistry, Rutgers-The State University of New Jersey, New Brunswick, New Jersey 08903.* *Received January 11, 1982*

**Abstract:** The $^1L_b$ two-photon spectra of second-row substituted benzenes, F, OH, and $NH_2$, are examined. The spectrum of phenol, which is reported for the first time, shows a mixture of Franck–Condon (FC) (allowed) and vibronic coupling (forbidden) character, in contrast to fluorobenzene and aniline which show very weak and very strong FC character, respectively. Perturbation theory treatment of the problem indicates that the degree of allowedness in the spectrum (though all are formally allowed by symmetry) is measured by resonance interaction of the substituent with the ring. This results from introduction of charge-transfer character into the intermediate and final state wave functions in the two-photon tensor. The potential field effect of the substituent (i.e., the inductive effect) is found to play only a minor role in inducing two-photon intensity unlike one-photon spectra where this effect dominates. The two-photon intensities are thus a direct measure of the resonance strength of chemical bonds.

## I. Introduction

It has taken nearly two decades for the regularities in molecular two-photon (TP) spectra to begin to become clear since Abella's initial observation of the TP spectrum in atomic cesium.[1] The large differences between normal optical; i.e., one-photon (OP), and TP spectra show the power of TP spectroscopy for studying molecular excited states. For example, TP spectra of linear polyenes demonstrate the existence of a previously unobserved (OP forbidden) low-lying state which might account for the photochemistry of these molecules.[2] And despite the many OP studies of the spectrum of benzene, definitive assignment of the 2600-Å absorption to the $^1B_{2u} \leftarrow {}^1A_{1g}$ transition was only finally made by TP spectroscopy.[3,4] The benzene spectrum indicates that the accepted norms of OP spectroscopy are not carried over to TP absorption. An example is found in the effect of deuterium perturbations, which is insignificant except for frequency shifts in OP absorption, but reveals new heretofore unobserved modes in the TP spectra.[5] The TP spectrum also allows studies such as Doppler-free rotational spectra (which has indicated that the benzene $^1B_{2u}$ excited state is not planar[6]) and on the changes of the normal coordinates on going to the excited state.[7,8] These studies are either difficult or impossible in OP absorption but are made possible because of the nature of TP transitions.

In this paper we exploit the dependence of the TP substituted benzene $^1L_b \leftarrow {}^1A$[9] transition tensor on resonance contributions to study valence interactions for the second-row substituents, F, OH, and $NH_2$. There have been many studies of substituent effects on benzene spectra, but as we will show in this example, TP spectroscopy provides a powerful approach for examining the resonance contribution to chemical bonding.

## II. Basic Ideas

The TP selection rules derive from the three basic terms in the TP transition amplitude:[10,11] (i) a (symmetric) scalar term which requires transitions between states of identical symmetry; (ii) a symmetric tensor term which follows selection rules appropriate for electric quadrupole transitions; (iii) an antisymmetric tensor term which obeys selection rules appropriate for magnetic dipole transitions but is zero in a one laser experiment which employs photons of identical frequency and polarization (i.e., as in our experiments). This should be compared to the OP transition amplitude which follows selection rules appropriate for electric dipole transitions. Only transitions between states of the same parity are allowed in TP spectroscopy, compared to the opposite in OP. Thus, from the $A_{1g}$ ground state of benzene, a TP transition to the near-ultraviolet $B_{2u}$ state is parity forbidden. Only by mixing g-parity electronic states into $B_{2u}$ can the TP transition show allowed character.

We will employ states in a perturbation scheme as zeroth-order levels (rather than orbitals or configurations) and show that the TP spectral intensities of substituted benzenes can be understood in terms of resonance interactions of the substituent,[12] i.e., the tendency for an electron of the substituent group to enter into conjugation with the benzene $\pi$ electrons.[13] In the case of sec-

(1) I. D. Abella, *Phys. Rev. Lett.*, **9**, 453 (1962).
(2) L. A. Heimbrook, J. E. Kenny, B. E. Kohler, and G. W. Scott, *J. Chem. Phys.*, **75**, 4338 (1981), and references therein.
(3) L. Wunsch, F. Metz, H. J. Neusser, and E. W. Schlag, *J. Chem. Phys.*, **66**, 386 (1977), and references therein.
(4) D. M. Friedrich and W. M. McClain, *Chem. Phys. Lett.*, **32**, 541 (1975).
(5) L. Goodman and R. P. Rava in "Advances in Laser Spectroscopy", Vol. 1, B. A. Garetz and J. R. Lombardi Eds., Heyden, Philadelphia, 1982, pp 21–53.
(6) E. Riedle, H. J. Neusser, and E. W. Schlag, *J. Chem. Phys.*, **75**, 4231 (1981).
(7) W. Hampf, H. J. Neusser, and E. W. Schlag, *Chem. Phys. Lett.*, **46**, 406 (1977).
(8) R. P. Rava and L. Goodman, *J. Phys. Chem.*, **86**, 480 (1982).
(9) Notation of J. R. Platt, *J. Chem. Phys.*, **17**, 484 (1949).
(10) F. Metz, W. E. Howard, L. Wunsch, H. J. Neusser, and E. W. Schlag, *Proc. R. Soc. London, Ser. A*, **363**, 381 (1978).
(11) (a) W. M. McClain, *J. Chem. Phys.*, **55**, 2789 (1971); (b) P. R. Munson and W. M. McClain, *ibid.*, **53**, 29 (1969). (c) W. M. McClain, and R. A. Harris, "Excited States", Vol. 3, E. C. Lim, Ed., Academic Press, New York, 1977, pp 2–56.
(12) L. Goodman and R. P. Rava, *J. Chem. Phys.*, **74**, 4826 (1981).
(13) J. N. Murrell, "The Theory and Electronic Spectra of Organic Molecules", Wiley, New York, 1963, p 190.

0002-7863/82/1504-3815$01.25/0 © 1982 American Chemical Society

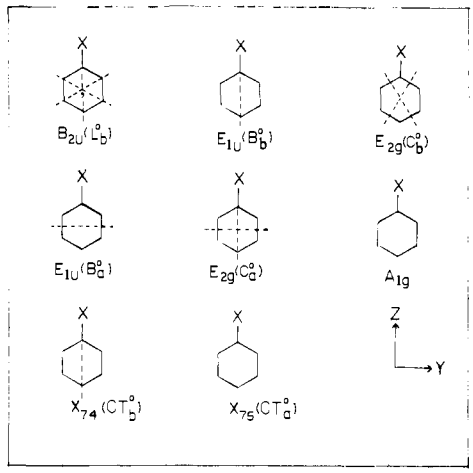


**Figure 1.** Nodal properties of the important zeroth-order excited states entering the intensity mechanism for the two-photon $^1L_b \leftarrow {}^1A$ transition in electrostatically perturbed benzenes. The first six diagrams are for locally excited benzenes states, the $A_{1g}$ one representing a two-electron excitation. $\chi_{74}$ ($CT_b^0$) and $\chi_{75}$ ($CT_a^0$) denote charge-transfer states generated by $\Phi_4 \leftarrow \Phi_7$ and $\Phi_5 \leftarrow \Phi_7$ excitations (Table II), respectively.

ond-row (donor) substituents, this is directly measured by the charge-transfer (CT) component of the wave function arising from the transfer of an electron out of the substituent lone pair to the benzene vacant orbitals. We first sketch the general ideas and fill in details in complete derivations in subsequent sections.

The $L_b$ transitioin (we adopt the Platt notation[9] as being appropriate for substituted benzene states) arises from the OP symmetry-forbidden $^1B_{2u} \leftarrow {}^1A_{1g}$ transition in benzene (i.e., as shown in Figure 1, there are three nodes in the $B_{2u}$ wave function instead of the required one) and derives its intensity in $C_6H_6$ for both OP and TP spectra entirely through vibronic interactions.[3,4,14] The addition of a substituent lowers the molecular symmetry from $D_{6h}$ to $C_{2v}$[15] and makes the transition formally allowed. However for many substituents, the excitation is largely localized in the $\pi$ system of the ring and the transition retains a similarity to that in benzene, i.e., basically weak with important amounts of vibronic intensity borrowing. The degree of allowedness gives a measure of the amount of interaction between the $\pi$ system of the ring and the substituent. Thus one expects a correlation between the resonance effect and the Franck–Condon (FC) intensity.

The OP transition moment to the $L_b$ state is

$$\mathbf{M}_y = \langle A|\mu_y|L_b\rangle \qquad (1)$$

involving a short ($y$) axis transition.[16,17] Contamination of the $L_b$ wave function by CT states (i.e., the resonance effect) is not effective in contributing intensity to the $L_b$ transition because short axis CT transitions, e.g., $CT_b^0$ in Figure 1, are weak (the excited-state orbital having a node through the carbon atom to which the substituent is attached). Instead the OP transition moment grows primarily through contamination of the $L_b$ wave function by $B_b^0$ states[18] (we denote unperturbed states by zero). This is illustrated in Figure 1 where superposition of the nodal diagrams for $L_b^0$ and $B_b^0$ reduces the nodes in $L_b$ to one.

The two-photon symmetric tensor (combining (i) and (ii) discussed above) for the absorption f ← g involving identical photons[10,11] is

$$(S_{\rho,\sigma})_{f,g} = \sum_i \left[\frac{1}{\Delta E_{ig} - \hbar\omega}\right][\langle g|\mu_\rho|i\rangle\langle i|\mu_\sigma|f\rangle + \langle g|\mu_\sigma|i\rangle\langle i|\mu_\rho|f\rangle] \qquad (2)$$

where i runs over virtual intermediate states, $\mu_\sigma$ or $\mu_\rho$ are the appropriate electric dipole components, $\rho, \sigma = x, y, z$, $\hbar\omega$ is the laser energy, and $\Delta E_{ig}$ is the energy difference between the ground and intermediate states. For monosubstituted benzenes of $C_{2v}$ symmetry, $S_{\rho\sigma}$ involves only the in-plane $S_{yz}$ components for a transition to the $B_2$ symmetry $L_b$ state. Then

$$S_{yz} = \sum_i \left[\frac{1}{\Delta E_{ig} - \hbar\omega}\right][\langle A_1|\mu_y|i\rangle\langle i|\mu_z|B_2\rangle + \langle A_1|\mu_z|i\rangle\langle i|\mu_y|B_2\rangle] \qquad (3)$$

For simplicity we consider as the one dominant intermediate state (i), for substituent groups having high-lying locally excited states, the $B_{a,b}$ state derived from the very strong vacuum ultraviolet $^1E_{1u} \leftarrow {}^1A_{1g}$ (V ← N) transition in benzene, which splits into $A_1$ ($B_a$) and $B_2$ ($B_b$) components in $C_{2v}$ symmetry (Figure 1) (i.e., we initially ignore the C and C′ states). Thus $S_{yz}$ becomes

$$S_{yz} = \left[\frac{1}{\Delta E - \hbar\omega}\right][\langle A|\mu_z|B_a\rangle\langle B_a|\mu_y|L_b\rangle + \langle A|\mu_y|B_b\rangle\langle B_b|\mu_z|L_b\rangle] \qquad (4)$$

where $\Delta E_{ig}$ has been replaced by $\Delta E$, the average energy of the split $E_{1u}$ state. Equation 4 is illustrated in Figure 2a showing that the $B_{a,b}^0 \leftrightarrow L_b^0$ factor vanishes in benzene iteself due to parity considerations consistent with the forbidden nature of the TP trnasition to $^1B_{2u}$. However, we see that this tensor contains a long axis ($z$) transition moment to $L_b$, $\langle B_b|\mu_z|L_b\rangle$ (in contrast to OP which only contains the short axis moment $\langle A|\mu_y|L_b\rangle$). The CT configuration, $CT_b^0$ (Figure 1), contaminating the $L_b^0$ and $B_b^0$ wave functions is very effective in inducing allowed TP intensity to the $L_b$ state, as will be shown in section IV. At the same time, as is demonstrated in section III, the TP tensor remains insensitive to the potential effect of the substituent. The electrostatic potential effect on $L_b$ mainly comes in through $B_b^0$ contamination, but this is ineffective in TP spectroscopy because of parity considerations. *The power of TP spectroscopy of the $L_b$ state in probing resonance interactions lies in just this point: its sensitivity to CT character and insensitivity to the inductive effect.*[12]

## III. Inductive Effect

We continue to follow the perturbation approach we have used previously[12] to develop eq 4. The bases are as follows: (i) only $\pi$-electron states are taken into account; (ii) the perturbations are considered small enough to neglect interactions with the ground state; (iii) the sum over intermediate states in eq 3 is restricted to the single strongly allowed $E_{1u}$ ($B_{a,b}^0$) state of benzene. The wave functions were classified in terms of mixing of $C_6H_6$ states, e.g.

$$\psi_{L_b} = \lambda(L_b)\psi_{L_b}^0 + \lambda(B_b)\psi_{B_b}^0 + \lambda(C_b)\psi_{C_b}^0 + \lambda(C_b')\psi_{C_b'}^0 + \lambda(CT)\psi_{CT_b}^0 \qquad (5)$$

where the states, $\psi^0$, expressed in terms of configurations, $\chi$, are given in Table I by using the molecular orbital numbering given in Table II. We termed $1 >> \lambda^2(B_b) >> \lambda^2(j)$ (j denotes other coupling states) the weak coupling case, $1 >> \lambda^2(j) \sim \lambda^2(B_b)$ the intermediate coupling case, and $\lambda^2(L_b) << 1$ the strong coupling case; i.e., the state $\psi_{L_b}$ is no longer benzene analogue. Analogous expressions for $\psi_{B_b}$, $\psi_{B_a}$ and $\psi_{L_a}$ can also be written. Our previous derivation of the lack of effectiveness of the inductive perturbation on the $L_b$ TP transition was in terms of the weak coupling limit. We now show that the same result derives from the intermediate coupling case *for the $L_b$ state.*

In developing eq 4 only the linear terms in $\lambda(j)$ need be retained for the weak and intermediate coupling cases, the square terms

(14) (a) M. Goeppert-Mayer and A. L. Sklar, *J. Chem. Phys.*, **6**, 645 (1938); (b) H. Sponer, G. Nordheim, A. L. Sklar, and E. Teller, *ibid.*, **7**, 207 (1939).

(15) For simplicity we neglect the deviations from $C_{2v}$ present in phenol and aniline.

(16) $z$ is taken as the ring-substituent (long) axis, $y$ is taken as the short axis, and $x$ is taken as the out-of-plane axis.

(17) R. S. Mulliken, *J. Chem. Phys.*, **23**, 1997 (1955).

(18) (a) J. N. Murrell and H. C. Longuet-Higgins, *Proc. Phys. Soc., London*, **68**, 329 (1955); (b) L. Goodman and H. Shull, *J. Chem. Phys.*, **27**, 1388 (1957).

Table I. Zeroth-Order Excited-State Wave Functions[a]

| | |
|---|---|
| $\psi L_b^0 = 2^{-1/2}[\chi_{25} + \chi_{34}]$ | $\psi C'_a{}^0 = \chi_{15}$ |
| $\psi B_b^0 = 2^{-1/2}[\chi_{25} - \chi_{34}]$ | $\psi C'_b{}^0 = \chi_{14}$ |
| $\psi L_a^0 = 2^{-1/2}[\chi_{24} - \chi_{35}]$ | $\psi L'_a{}^0 = \chi_{16}$ |
| $\psi B_a^0 = 2^{-1/2}[\chi_{24} + \chi_{35}]$ | $\psi CT_b{}^0 = \chi_{74}$ |
| $\psi C_a^0 = \chi_{36}$ | $\psi CT_a{}^0 = \chi_{75}$ |
| $\psi C_b^0 = \chi_{26}$ | $\psi CT_a{}^0 = \chi_{76}$ |

[a] $\chi_{ij}$ represents the configurational wavefunction generated by the promotion $\Phi_i \rightarrow \Phi_j$. The molecular orbitals are given in Table II.

Table II. Molecular Orbital Numbering[a,b]

$\Phi_1 = (1/6^{1/2})(\phi_1 + \phi_2 + \phi_3 + \phi_4 + \phi_5 + \phi_6)$
$\Phi_2 = (1/4^{1/2})(\phi_2 + \phi_3 - \phi_5 - \phi_6)$
$\Phi_3 = (1/12^{1/2})(2\phi_1 + \phi_2 - \phi_3 - 2\phi_4 - \phi_5 + \phi_6)$
$\Phi_4 = (1/4^{1/2})(\phi_2 - \phi_3 + \phi_5 - \phi_6)$
$\Phi_5 = (1/12^{1/2})(2\phi_1 - \phi_2 - \phi_3 + 2\phi_4 - \phi_5 - \phi_6)$
$\Phi_6 = (1/6^{1/2})(\phi_1 - \phi_2 + \phi_3 - \phi_4 + \phi_5 - \phi_6)$
$\Phi_7 = \phi_7$

[a] $\phi_i$ represents a $2p\pi$ atomic orbital centered on atom $i$. [b] The substituent $\pi$ orbital containing atom 7 is bonded to carbon 1. Numbering is clockwise from carbon 1.

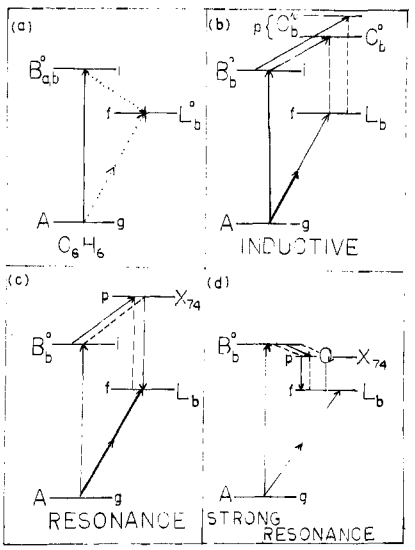


**Figure 2.** Principal mechanisms for two-photon intensity showing how the transition becomes ($yz$) electric quadrupole allowed by substitution. g, f, and i represent the ground, final, and intermediate states entering the transition tensor (eq 2), and p represents the most important contaminating (perturbing) state(s) introduced by the substituent with the dashed line showing nonvanishing perturbation matrix elements. The arrow indicates electric dipole, and the double arrow electric quadrupole matrix elements of the light field, and the dotted line forbidden transitions. In the strong resonance case (d), the square term of eq 14 becomes important and Q represents the contribution of the CT state dipole moment, $\mu_{CT}^0$.

becoming important solely for strong coupling. Consider the inductive effect of a substituent explicitly. The inductive effect allows the TP transition by mixing the g-parity states of Figure 1 into $L_b$ through the substituent modifying the potential acting on the benzene $\pi$ electrons. There are two $E_{2g}$ states ($C_{a,b}^0$ and $C'_{a,b}{}^0$) which may mix into $L_b^0$ and $B_{a,b}^0$. The state perturbation matrix elements in terms of the MO's of Table II are

$$\langle L_b^0|H|B_b^0\rangle = {}^1/_2[\langle\Phi_5|H|\Phi_5\rangle + \langle\Phi_3|H|\Phi_3\rangle - \langle\Phi_2|H|\Phi_2\rangle - \langle\Phi_4|H|\Phi_4\rangle] \approx {}^1/_3\delta_1 \quad (6)$$

$$\langle L_b^0|H|C_b^0\rangle = \langle B_b^0|H|C_b^0\rangle = \langle B_a^0|H|C_a^0\rangle = (1/2^{1/2})\langle\Phi_5|H|\Phi_6\rangle \approx {}^1/_6\delta_1$$

$$\langle L_b^0|H|C'_b{}^6\rangle = -\langle B_b^0|H|C'_b{}^0\rangle = \langle B_a^0|H|C'_a{}^0\rangle = -(1/2^{1/2})\langle\Phi_1|H|\Phi_3\rangle \approx -{}^1/_6\delta_1$$

$$\langle L_b^0|H|CT_b^0\rangle = \langle B_b^0|H|CT_b^0\rangle = \langle B_a^0|H|CT_a^0\rangle = \langle B_a^0|H|CT'_a{}^0\rangle \approx 0$$

where $\delta_r = \langle\phi_r|H|\phi_r\rangle$ ($\phi_r$ are atomic orbitals). The only inductive perturbation matrix element, $\delta_r$, retained in eq 6 is the perturbation on the substituted ring carbon ($r = 1$).

For the weak and intermediate coupling cases the inductive effect yields the perturbation wave functions

$$\psi_{L_b} = \psi_{L_b}{}^0 + \lambda(B_b)\psi_{B_b}{}^0 + \lambda(C_b)\psi_{C_b}{}^0 + \lambda(C_b')\psi_{C'_b}{}^0 \quad (7a)$$

$$\psi_{B_b} = \psi_{B_b}{}^0 + \Lambda(L_b)\psi_{L_b}{}^0 + \Lambda(C_b)\psi_{C_b}{}^0 + \Lambda(C'_b)\psi_{C'_b}{}^0 \quad (7b)$$

$$\psi_{B_a} = \psi_{B_a}{}^0 + l(L_a)\psi_{L_a}{}^0 + l(C_a)\psi_{C_a}{}^0 + l(C'_a)\psi'_{C'_a}{}^0 \quad (7c)$$

When substituted into eq 4, these wave functions give the formidable appearing expression

$$S_{yz} = \left[\frac{1}{\Delta E - \hbar\omega}\right][\langle A^0|\mu_z|B_a^0\rangle\{l(C_a)\langle C_a^0|\mu_y|L_b^0\rangle + l(C'_a)\langle C'_a{}^0|\mu_y|L_b^0\rangle + \lambda(C_b)\langle B_a^0|\mu_y|C_b^0\rangle + \lambda(C'_b)\langle B_a^0|\mu_y|C'_b{}^0\rangle\} + \langle A^0|\mu_y|B_b^0\rangle\{\Lambda(C_b)\langle C_b^0|\mu_z|L_b^0\rangle + \Lambda(C'_b)\langle C'_b{}^0|\mu_z|L_b^0\rangle + \lambda(C_b)\langle B_b^0|\mu_z|C_b^0\rangle + \lambda(C'_b)\langle B_b^0|\mu_z|C'_b{}^0\rangle\}] \quad (8)$$

However, the individual electric dipole transition moments $\langle A^0|\mu_z|B_a^0\rangle$ etc. as tabulated in Table III make eq 8 conceptually useful, i.e.

$$S_{yz} = \left[\frac{1}{\Delta E - \hbar\omega}\right]8^{-1/2}R^2\mathbf{jk}[-l(C_a) - l(C'_a) - \Lambda(C_b) + \Lambda(C'_b) - 2\lambda(C_b) - 2\lambda(C'_b)] \quad (9)$$

The mixing coefficients $\lambda(C)$, $\Lambda(C)$, and $l(C)$ depend linearly on the perturbation matrix element and inversely on the energy separation between the states. Thus incorporating the sign relationships of eq 6 into eq 9 and recalling that $C_a^0$ and $C_b^0$, and $C'_a{}^0$ and $C'_b{}^0$ are degenerate yields

$$S_{yz} = \frac{-2^{-1/2}R^2}{\Delta E - \hbar\omega}\mathbf{jk}\{[\lambda(C_b) + \lambda(C'_b)] + [\Lambda(C_b) - \Lambda(C'_b)]\} \quad (10)$$

If we also consider the C and C′ states as additional possible intermediate states in eq 4, we find the $(\Lambda(C_b) - \Lambda(C'_b))$ term nearly cancels with the new terms generated by these intermediate states, leaving only $\lambda(C_b) + \lambda(C'_b)$. The sign relations in (6), $\lambda(C_b) > 0$, $\lambda(C'_b) < 0$, show that contaminating terms to the excited $L_b$ state strongly cancel. Thus, the perturbation theory development of eq 4 gives rise to weak FC intensity primarily through the mechanism depicted in Figure 2b;i.e., perturbation of the excited $L_b$ state is dominant.

The value of $\delta_r$ for external substituents to the ring probably never exceeds ~1 eV,[18] and since the $C_{a,b}^0$ state has been placed[19] near 60 000 $cm^{-1}$, some 3 eV above $L_b$, the values of $\lambda(C_b)$, $\lambda(C'_b) < 0.1$. *The important conclusion is that the inductive effect will be ineffective in imparting intensity to the $L_b$ TP spectrum.*

In contrast to the out-of-phase contamination of $L_b^0$ by $C_b^0$ and $C'_b{}^0$ involving the TP mechanism of Figure 2b, the combination of large matrix element and smaller energy gap between $L_b^0$ and $B_b^0$ accounts for the higher sensitivity of the OP spectrum to inductive type perturbations. The consequence is that the inductive effect can in general be associated with strong and weak FC components of OP and TP spectra, respectively. Substantial confirmation of this prediction has recently been obtained by Callis, Scott, and Albrecht's study of the TP $L_b$ spectrum of the 1,3-diazine (pyrimidine) in solution,[20] showing that despite formal

(19) J. Philis, A. Bolovinos, G. Andritsopoulos, E. Pantos, and P. Tsekeris, *J. Phys. B.*, **14**, 3621 (1981).
(20) P. R. Callis, T. W. Scott, and A. C. Albrecht, *J. Chem. Phys.*, **75**, 5640 (1981).

Table III. Electric Dipole Matrix Elements[a-c]

| $^1/_2R$j | $^1/_2R$k | $-^1/_2R$j | $-^1/_2R$k | $-6^{1/2}/4RS$k |
|---|---|---|---|---|
| $\langle B_b^0\|\mu_y\|C_a^0\rangle$ | $2^{-1/2}\langle A^0\|\mu_z\|B_a^0\rangle$<br>$\langle B_a^0\|\mu_z\|C_a^0\rangle$<br>$\langle B_b^0\|\mu_z\|C_b^0\rangle$<br>$\langle B_b^0\|\mu_z\|C'_b{}^0\rangle$<br>$\langle C_b^0\|\mu_z\|L_b^0\rangle$ | $2^{-1/2}\langle A^0\|\mu_y\|B_b^0\rangle$<br>$\langle B_a^0\|\mu_y\|C_b^0\rangle$<br>$\langle C_a^0\|\mu_y\|L_b^0\rangle$<br>$\langle C'_a{}^0\|\mu_y\|L_b^0\rangle$<br>$\langle B_a^0\|\mu_y\|C'_b{}^0\rangle$<br>$\langle B_b^0\|\mu_y\|C'_a{}^0\rangle$ | $\langle B_a^0\|\mu_z\|C'_a{}^0\rangle$<br>$\langle C'_b{}^0\|\mu_z\|L_b^0\rangle$ | $\langle L_b^0\|\mu_z\|CT_b^0\rangle$<br>$\langle B_a^0\|\mu_z\|CT_a^0\rangle$<br>$\langle B_b^0\|\mu_z\|CT_b^0\rangle$<br>$\langle C'_b{}^0\|\mu_z\|CT_b^0\rangle$<br>$\langle C'_a{}^0\|\mu_z\|CT_a^0\rangle$ |

[a] All bond distances are assumed to be $R$. $S$ is the overlap integral between $\pi$ orbitals on atoms 1 and 7. [b] k is a unit vector along the substituent–ring (1–7) axis; j is along the short ($y$) molecular axis. [c] Phases are determined by the molecular orbitals given in Table II.

allowedness, the primary mechanism for intensity remains vibronic coupling, analogous to that in benzene. Strong TP bands are then expected only for heterocyclic substitution by very electronegative atoms, possibly oxygen.

While the formal theory for the as yet unobserved TP $L_a$ and $B_{a,b}$ spectra of benzene and its derivatives has parallel features, there are important differences. One is that the smaller energy gap between $C_a^0$, $C'_a{}^0$, and these higher lying states will cause the contaminations to be larger. Another is the different phasing in the transition tensors for the $L_a$ and $B_b$ states. These differences along with failure of the Born–Oppenheimer approximation for high energy states may cause the perturbation model that we are using for the $L_b$ state to become invalid and should result in greater sensitivity of the TP strength of these transitions to inductive perturbations.

## IV. Resonance Effect

The resonance effect is described as the ability of a substituent to extend the space over which the $\pi$ electrons are delocalized.[13,21] This is exemplified by admixture of the CT state $CT_b^0$ into $L_b^0$ and $B_b^0$ and $CT_a^0$ into $B_a^0$ (Figure 1). (We ignore the C and C′ states in our treatment for simplicity even though their inclusion will give additional terms[12]). Since in the paradigm situation that we are visualizing there is no modification of the potential acting on the benzene $\pi$ electrons, perturbation matrix elements over ring states vanish. Thus, to the first order the perturbed wave functions become

$$\psi_{L_b} = \psi_{L_b}{}^0 + \lambda(CT)\psi_{CT_b}{}^0 \quad (11a)$$

$$\psi_{B_b} = \psi_{B_b}{}^0 + \Lambda(CT)\psi_{CT_b}{}^0 \quad (11b)$$

$$\psi_{B_a} = \psi_{B_a}{}^0 + l(CT)\psi_{CT_a}{}^0 \quad (11c)$$

Equation 4 now takes the form[22]

$$S_{yz} = \left[\frac{1}{\Delta E - \hbar\omega}\right][\langle A^0|\mu_z|B_a\rangle\{l(CT)\langle\chi_{75}|\mu_y|L_b{}^0\rangle + \lambda(CT) \times \langle B_a{}^0|\mu_y|\chi_{74}\rangle\} + \langle A^0|\mu_y|B_b{}^0\rangle\{\Lambda(CT)\langle\chi_{74}|\mu_z|L_b{}^0\rangle + \lambda(CT)\langle B_b{}^0|\mu_z|\chi_{74}\rangle\}] \quad (12)$$

All short axis ($y$) polarized transitions moments involving the CT configuration may be ignored since these are negligible compared to the long-axis ones. Hence

$$S_{yz} = \frac{2^{-1/2}}{\Delta E - \hbar\omega}[\langle A^0|\mu_y|B_b{}^0\rangle\{\Lambda(CT)\langle\Phi_7|\mu_z|\Phi_3\rangle - \lambda(CT)\langle\Phi_7|\mu_z|\Phi_3\rangle\}] \quad (13)$$

The perturbation matrix elements of the interaction between the CT and benzene locally excited states in (11) are in each case $(\pm 6^{-1/2})\beta$, where $\beta$ is the resonance integral associated with the benzene–substituent bond. Thus the two mixing coefficients in (13) have the forms $(\pm 6^{-1/2})\beta(\Delta E_i{}^0)^{-1}$. An illustration of the magnitudes of $\lambda$(CT) and $\Lambda$(CT) can be obtained from estimates of $\beta \approx -1.2$ eV and of $\Delta E_{CT_b}{}^0 \approx 8$ eV for phenol.[21,23,24] These quantities along with 4.9 eV, the experimental value for $\Delta E_{L_b}{}^0$, give $\lambda(CT) \approx 0.2$ and $\Lambda(CT) \approx -0.4$.

It only remains to estimate $\langle\Phi_7|\mu_z|\Phi_3\rangle$. This represents a long axis electric dipole transition moment between a ring and substituent orbital and its magnitude is approximately $(3^{1/2}/2)RS$ where $S$ is the C–X bond overlap integral and R is the average of C–C and C–X bond lengths. Since $S$ for the second row is $\approx$0.2,[24] the TP spectrum in the case of a resonance perturbating substituent, is expected to have significant contributions from the CT states (Figure 2c). These are expected to be small for fluoro[25] (where the $\pi$ lone pair is tightly bound) and important for hydroxy (where it is more diffuse) with the consequence that the FC part of the TP spectrum will be appreciable in the latter case. The FC intensity will reflect the magnitudes of both the $\Lambda$(CT) and $\lambda$(CT) terms in eq 13, which add constructively because $\Lambda$(CT) and $\lambda$(CT) have opposite signs in the intermediate coupling case (where the CT state is high lying). In general, $\Lambda$(CT) will exceed $\lambda$(CT); however, both of the terms are expected to be important.

If the energy of the CT configuration is low enough, as in aniline, where $\Delta E_{7\to4}{}^0$ is only $\sim$6 eV,[21,24] perturbation theory breaks down. The benzene and CT states become scrambled, and the linear transition tensor (eq 13) is no longer valid. The strong coupling (Figure 2d) implied by this case is further discussed in section VII. However, the general consequences are that OP and TP spectra will resemble each other to a considerable extent and that the TP FC strength will be high.

For second-row substituents the magnitude of resonance-induced mixing is large enough to categorize the $L_b$ states as examples of the intermediate or strong coupling cases. The consequent resonance induced TP intensity will outweight any contribution from the inductive effect. *The major conclusion is that unlike the inductive effect, resonance interactions have the potentiality for imparting large intensity to the $L_b$ TP spectrum.*

## V. Experimental Details

The TP spectra were obtained by vapor fluorescence excitation (FE). Aniline, chlorobenzene, and bromobenzene (MCB, spectrophotometric grade) were purified by repeated distillation; phenol (Fisher, laboratory grade) was purified by repeated vacuum sublimation; fluorobenzene (Aldrich, 99%) was used as supplied. All compounds were degassed and sublimed or distilled into a previously evacuated ($<10^{-2}$ torr) 15-mm quartz suprasil cell until they reached their room-temperature equilibrium vapor pressure.

A DL16 Molectron dye laser pumped by the third harmonic (355 nm) of a MY 32 Molectron Nd:YAG laser (focused by a 150-mm focal length lens into the cell) provided the excitation. The dye laser was operated in the fifth order with dyes C500, C540A, R590, and R610 (Exciton, in ethanol) at a minimum scan speed of 2 Å/min. The resulting wavenumber accuracy is $\pm$3 cm$^{-1}$ (OP energy). The peak laser energy ranged from 400 to 700 $\mu$J/pulse before focusing. Fluorescence was monitored at 90° to the laser beam by a radio frequency shielded 1P28B phototube filtered from laser light by 6 mm of Corning CS7-54 filters, and the intensity of the laser light measured by a Si photodiode. The outputs of the phototube and photodiode were processed through separate channels of a PAR 162/164/165 boxcar integration system which corrected the

(21) J. N. Murrell, *Proc. Phys. Soc., London*, **68**, 969 (1955).

(22) At first thought it might appear that the additional intermediate states $CT_a$ and $CT_b$ might be important. However, $CT_b$ is ineffective because short axis CT transitions are weak and $CT_a$ is ineffective because it generates the matrix element $\langle CT_a|\mu_y|L_b{}^0\rangle$. When expanded over eq 11, this reduces to terms of the sort $\langle CT_a{}^0|\mu_y|CT_b{}^0\rangle$, $\langle B_a{}^0|\mu_y|L_b{}^0\rangle$, etc., all of which vanish or are small.

(23) Estimated from $\Delta E_{CT_b}{}^0 \approx I - A - 5$ eV., where $A$ is the electron affinity of benzene (–0.5 eV) and $I$ is the ionization potential of OH (12.6 eV).[24]

(24) Reference 13, p 221.

(25) A similar calculation[21] to that carried out for phenol gives $\lambda(CT) = 0.09$ and $\Lambda(CT) = 0.14$.

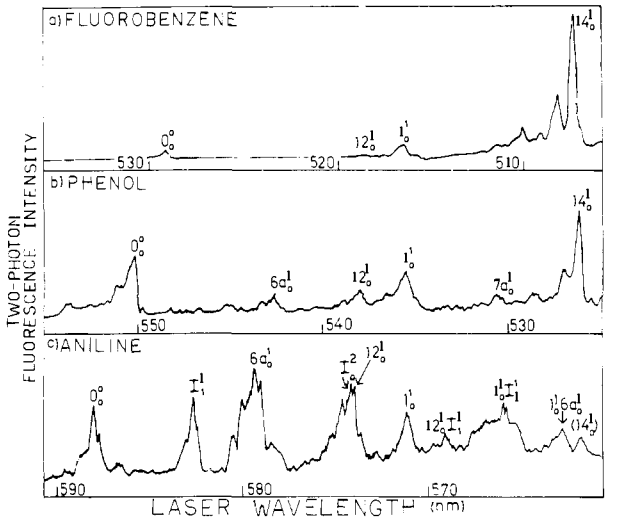


**Figure 3.** The fundamental region of the two-photon vapor fluorescence excitation spectra to the $^1L_b$ state of (a) fluorobenzene, (b) phenol, and (c) aniline. The band $14_0^1$ in each case represents the vibronic coupling part of the spectrum and is believed to be of approximately equal intensity.[5] The Franck–Condon (allowed) portion is directly measured by the $0_0^0$, $1_0^1$, and $6a_0^1$ strengths.

Table IV. Two-Photon Absorptivities[a] ($\delta$ in cm$^4$ s mol$^{-1}$ photon$^{-1}$), One Photon Oscillator Strengths[b] and 0-0 Band Wavenumbers

| molecule | $\delta$(0-0) | $\delta(1_0^1)$ | $f$ | $\tilde{\nu}_{0-0}$ |
|---|---|---|---|---|
| benzene | 0 | 0 | 0 | 38 086 |
| fluorobenzene | $5 \times 10^{-51}$ | $7 \times 10^{-51}$ | 0.009 | 37 816 |
| phenol | $7 \times 10^{-50}$ | $4 \times 10^{-50}$ | 0.02 | 36 344 |
| aniline | $5 \times 10^{-49}$ | $3 \times 10^{-49}$ | 0.03 | 34 032 |
| chlorobenzene | $5 \times 10^{-50}$ | $3 \times 10^{-50}$ | 0.002 | 37 176 |
| bromobenzene | $7 \times 10^{-50}$ | $6 \times 10^{-50}$ | 0.0015 | 36 996 |

[a] The TP absorptivity of the vibronic coupling band $14_0^1$ is assumed unchanged from that of benzene ($1 \times 10^{-49}$).[26] The vapor-phase absorptivities of the other bands are then determined by using $14_0^1$ as a standard. [b] From ref 27.

spectra to the square of laser intensity. Final plotting used a strip chart recorder. Hg line spectra, obtained by a Spex 1M 1704 spectrometer operating in the first order, were used for calibration. Spectra were run in both linearly polarized and circularly polarized light to aid in the assignments. These were obtained by using an intracavity polarizer and an Oriel 2760 circular polarizer, respectively.

Vapor-phase OP spectra were measured on a Cary Model 17 spectrophotometer with 0.5–1-Å resolutions.

## VI. The $^1L_b \leftarrow {}^1A$ Two-Photon Spectra

**A. Overview.** The fundamental regions of the 5000–6000-Å TP spectra for the $^1L_b(B_2) \leftarrow {}^1A(A_1)$ transition in fluorobenzene, phenol, and aniline are shown in Figure 3. The fluorobenzene spectrum has been thoroughly analyzed and will be only briefly discussed. This is the first report of the TP $^1L_b$ spectrum of phenol, and a complete analysis is given below. A portion of the aniline TP spectrum has been previously reported,[12] by using multiphoton ionization (MPI) techniques. However, while the MPI spectrum was overlapped by a Rydberg transition and cutoff at ~1000 cm$^{-1}$ above the origin, FE allows the analysis to be extended to higher energies. There can be no doubt that the spectra in Figure 3 correspond to the $^1L_b \leftarrow {}^1A$ transition since the origin bands at $2\tilde{\nu}$ are identical, within experimental error, with the OP origins (Table IV).[26-30]

Figure 3 reveals that there are strong differences between the TP spectra of these three molecules. The TP spectrum of fluorobenzene is mainly built on the $b_2$ vibronic coupling (VC) mode, $\nu_{14}$, with only a weak origin band and FC progressions in $\nu_1$, and

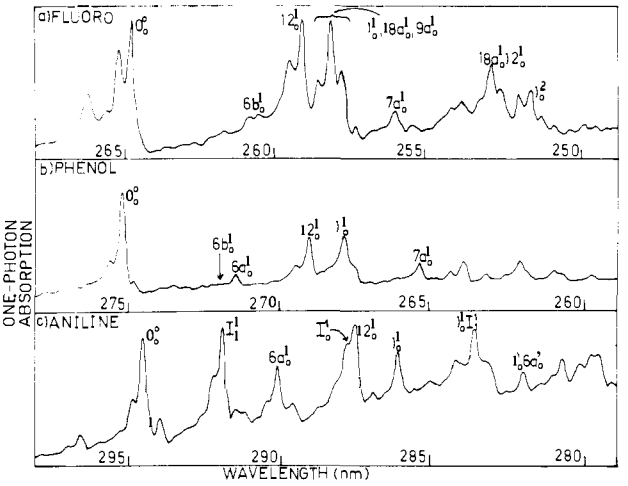


**Figure 4.** The fundamental region of the one-photon vapor absorption to the $^1L_b$ state of (a) fluorobenzene, (b) phenol, and (c) aniline. The band $6b_0^1$ in each case represents the vibronic coupling part of the spectrum. In aniline the FC part overwhelms $6b_0^1$.

Table V. Major Bands in the Two-Photon Vapor Spectrum of Phenol

| λ, Å | $2\tilde{\nu}$, cm$^{-1}$ | $\Delta\nu_{0-0}$ | intens | assignt[a] |
|---|---|---|---|---|
| 5535.0 | 36 124 | −220 | m | $16a_1^1$ |
| 5525.2 | 36 188 | −156 | w | $6a_1^1 6b_1^1$ |
| 5523.0 | 36 202 | −142 | w | |
| 5516.0 | 36 248 | −96 | w | $6b_1^1$ |
| 5511.0 | 36 280 | −64 | w | $6a_1^1$ |
| 5505.6 | 36 316 | −28 | m | $11_0^1$ |
| 5501.5 | 36 344 | 0 | vs | $0_0^1$ |
| 5500.0 | 36 354 | +10 | | *b* |
| 5499.3 | 36 358 | 14 | | *b* |
| 5471.5 | 36 552 | 208 | w | $11_0^1$ |
| 5432.0 | 36 808 | 464 | m | $6a_0^1$ |
| 5486.5 | 37 120 | 776 | m | $12_0^1$ |
| 5363.8 | 37 276 | 932 | s | $1_0^1$ |
| 5359.0 | 37 310 | 966 | m | $18a_0^1$ |
| 5315.0 | 37 618 | 1274 | m | $7a_0^1$ |
| 5274.0 | 37 912 | 1568 | vs | $14_0^1$ |

[a] Sequence satellites are only listed for the origin band. [b] Tentatively assigned as part of the rotational contour.

thus strongly resembles benzene. In dramatic contrast, the phenol spectrum has a strong 0–0 band, many active FC modes, and strong progressions in $\nu_1$, in addition to the active VC mode $\nu_{14}$. Finally, the aniline spectrum is strongly allowed, the FC bands overwhelming the VC ones. Comparison of the origin band strengths and total integrated FC intensities (Table IV) shows that the FC intensity in fluorobenzene is ~$10^{-1}$ of phenol and $10^{-2}$ of aniline.

On the other hand, the OP spectra shown in Figure 4 show that the spectrum in each case is strongly allowed[27-30] (the VC contribution is represented by the weak band $6b_0^1$) with the FC intensity for fluorobenzene approximately half that for phenol and about one-third that of aniline. Comparison of Figures 3 and 4 shows that the OP and TP spectra appear similar only for aniline.

**B. Vibrational Analysis. (1) Fluorobenzene.** The intensity ordering of the vibronic fundamental bands in the TP fluorobenzene spectrum is found to be: $14_0^1(b_2) >> 1_0^1(a_1) \gtrsim 0_0^0$ (origin band) $> 12_0^1(a_1) > 7a_0^1(a_1)$.[31-35] As in all benzenoid systems,

(26) R. M. Hochstrasser, G. R. Meredith, and H. P. Trommsdorf, *J. Chem. Phys.*, **73**, 1009 (1980).

(27) F. A. Matsen, *J. Am. Chem. Soc.*, **72**, 5243 (1950); W. W. Robertson and F. A. Matsen, *ibid.*, **72**, 5252 (1950).

(28) C. D. Lipp and C. J. Seliskar, *J. Mol. Spectrosc.*, **87**, 242, 255 (1982).

(29) H. D. Bist, J. C. D. Brand, and D. R. Willaims, *J. Mol. Spectrosc.*, **21**, 76 (1966); **24**, 402, 413 (1967).

(30) J. C. D. Brand, D. R. Willaims, and T. J. Cook, *J. Mol. Spectrosc.*, **20**, 359 (1966).

(31) The Wilson vibrational numbering[32] is used with the sub- and superscripts, giving the number of quanta in the ground and excited states, respectively.[30]

the spectrum is congested by low-lying sequence bands which build to the red of all the major bands with intensities (energy in $cm^{-1}$ is shown in parentheses) $18b_1^1$ (−17) > $11_1^1$ (−57) > $16a_1^1$ (−206) ≳ $16b_1^1$ (−168) ≳ $6b_1^1$ (−95) > $6a_1^1$ (−57). With the exception of some very weak bands and the appearance of $\nu_{18a}$ in combination bands, almost the entire spectrum to ~5000 $cm^{-1}$ above the origin can be generated by these fundamentals and sequences.

**(2) Phenol.** Since this is the first report of the TP $^1L_b$ phenol spectrum, the major bands are listed in Table V. Through phenol belongs to the $C_s$ point group, the barrier to rotation of the OH group is so small that the transition is well described by $C_{2v}$ symmetry designations. Detailed OP analysis of this band system has confirmed this as being accurate.[29]

The most intense band in the spectrum falls at 5274 Å and shows polarization behavior appropriate for a $b_2$ vibration. In analogy to the spectrum of benzene and other substituted benzenes, the polarization, intensity, and position of this band above the origin (+1568 $cm^{-1}$) require it to be assigned as $14_0^1$. Only this band and sequence bands built upon it show the polarization behavior of a $b_2$ vibration, and thus it is the only vibration of this symmetry observed.

The other fundamentals can all be correlated with OP absorption and are all $a_1$ modes. They are the following: $6a_0^1$ (+464), $12_0^1$ (+776), $1_0^1$ (+932), $18a_0^1$ (+966), and $7a_0^1$ (+1275). With the exception of the FC mode $6a_0^1$, these are the same modes which appear in the fluorobenzene spectrum. The significance of this observation will be discussed further in section VIC. All of these $a_1$ fundamentals appear strongly in combination with $\nu_{14}$ and with each other.

Low-lying sequence bands appear consistently clustered to the red of all strong bands. The fundamental sequences are $11_1^1$ (-28), $6a_1^1$ (−64), $6b_1^1$ (−96), and $16a_1^1$ (−220). The low-vapor pressure of phenol and unfavorable Boltzmann factors make analysis of the hot bands beyond -250 $cm^{-1}$ difficult.

Thus the phenol spectrum appears intermediate between a forbidden benzene VC spectrum and a fully FC allowed one. The fundamental intensity ordering is $14_0^1 > 0_0^0 > 1_0^1 > 12_0^1 > 6a_0^1 > 7a_0^1 > 18a_0^1$. The strongest band in the TP spectrum is still due to VC, involving the $b_2$ mode $\nu_{14}$.

**(3) Aniline.** As seen from Figure 3, the aniline $^1L_b$ TP spectrum cannot be correlated with other substituted benzene spectra. All the strong bands have $a_1$ vibrational symmetry. The entire spectrum can be mapped onto the observed OP spectrum, with the exception of a weak band at +1500 $cm^{-1}$ (labeled $14_0^1$ in Figure 3c). This might then represent the VC portion of the spectrum. Unfortunately, because of the weakness, polarization data is inconclusive and this assignment is tentative. In any case the VC spectrum is weak.

The active fundamental bands are all due to FC modes and follow the intensity ordering $6a_0^1 > 12_0^1 \approx 0_0^0 > 1_0^1$. This represents a change in ordering from that in the other substituted benzenes and will be discussed in the next section. The major sequence band is also different in aniline, arising from the inversion vibration about the nitrogen $I$, lying to the blue side of the major bands ($I_1^1$ = +294 $cm^{-1}$). The vibration is strongly anharmonic with a very intense first harmonic, $I_0^2$, at +758 $cm^{-1}$.

**C. The Franck–Condon Vibration $\nu_{6a}$.** We have seen that a rough comparison of the allowed FC character in the TP spectra of the $^1L_b \leftarrow {}^1A$ transition in monosubstituted benzenes offers an assessment of the resonance effect. In this section we show that a more careful examination of the FC vibronic intensities allows subtle features of the interaction of substituent groups to be revealed. OP spectroscopy reveals that the most important FC modes are the ring breathing vibration $\nu_1$ and the Kekulé mode $\nu_{12}$. Their activity is consistent with both ring contraction and unequal bond length changes on excitation.

Table VI. Relative Intensities of $6a_0^1$ and $12_0^1$ in Two-Photon Spectra of Fluorobenzene, Phenol, and Aniline

| molecule | (0-0) | ($6a_0^1$) | ($12_0^1$) |
|---|---|---|---|
| fluorobenzene | 10 | 0 | 0 |
| phenol | 140 | 35 | 45 |
| anisole | 140 | 15 | 45 |
| aniline | 1000 | 1200 | 800 |

The vibration of interest in the TP spectrum is the ring flattening mode $\nu_{6a}$. This mode is known to be substituent sensitive from infrared and Raman studies of halogen-substituted benzenes. In the TP absorption, the mode may only be active through FC effects. Comparison of the intensity of $6a_0^1$ in the different substituted benzenes should correlate with the degree of allowed character in the TP spectrum and consequently the resonance effect of the substituent. The reason that this mode is not commented on in OP absorption is that its intensity may arise from both FC and VC effects.

The relative intensity of $6a_0^1$ to the origin band in the TP spectra shows the following relationship for the second-row groups: $NH_2$ > OH >> F (Table VII). In fluorobenzene, this band is actually too weak to be observed, but it has significant intensity in phenol. The intensity of $6a_0^1$ in the TP spectrum of anisole, where the OH hydrogen is replaced by $CH_3$, is decreased significantly (Table VI), though the origin intensity and VC intensity, $14_0^1$, are comparable to phenol. Since the ionization potential of $OCH_3$ is lower than that of OH, the activity of $\nu_{6a}$ is revealed to be sensitive to the resonance integral. In aniline, $6a_0^1$ has become the most intense band consistent with strong resonance interaction. Thus TP spectroscopy reveals that ring flattening is also occurring on excitation and that this flattening parallels the resonance interaction of the substituent group.

## VII. Discussion

The weak coupling case (i.e., $\lambda_{B_b}^2$, $\Lambda_{L_b}^2$, and $l_{B_a}^2$ >> any other $\lambda^2$, $\Lambda^2$, or $l^2$) can be viewed as arising from first-order degenerate perturbation theory between the configurations $\chi_{24}^0$, $\chi_{25}^0$, $\chi_{34}^0$, and $\chi_{35}^0$. This case, although it explains the main features of OP spectroscopy, does not cause the forbidden TP $^1L_b$ transition in benzene to become allowed. The first-order corrections to the zeorth-order degenerate perturbation theory wave functions of the weak coupling case generate the intermediate coupling case. The TP $L_b$ transition becomes allowed and the transition tensor is linear in the CT mixing coefficients $\lambda$ and $\Lambda$. The breakdown of perturbation theory, so that the assumptions used to derive eq 8 are no longer valid, results in the strong coupling case. In particular, the square terms $\lambda^2$, $\lambda\Lambda$, etc. neglected in eq 8 become significant, and perturbation of the ground state may be important.

The perturbation theory estimates made in sections III and IV suggest that fluorobenzene and phenol fit into the intermediate coupling case and the spectra shown in section V confirms this view. A consequence of the intermediate coupling view is that the TP $L_b$ FC intensity measures resonance interactions with little interference from the inductive effect. This stems from the linear CT contributions to $L_b$ and $B_b$. A simple relationship can then be found between the FC intensity $\sim S_{yz}^2$, and the energy shift of the $L_b$ origin in the substituted benzene from the benzene $L_b^0$ origin, $\Delta^2E$. This follows from eq 11 and 13, taking into account that the matrix elements determining $\lambda$(CT) and $\Lambda$(CT) are identical except for sign (section IV). The result is that $\Delta^2E \approx \lambda(CT)_2\Delta^2E_{L_b}{}^0$ and $S_{yz}^2/\Delta^2E \approx (\Delta E - \hbar\omega)^{-1}[(\Delta^2E_{L_b}{}^0)^{-1} + \Delta^2E_{L_b}{}^0(\Delta^2E_{B_b}{}^0)^{-2} + 2(\Delta^2E_{b_b}{}^0)^{-1}]$. In the above relationships $\Delta^2E_i^0 \equiv \Delta E_{CT}^0 - \Delta E_i^0$. Since $\Delta E \approx (5\text{–}6) \times 10^{-4}$ $cm^{-1}$ and we excite with green to orange photons ($\hbar\omega \approx (1.7\text{–}2.0) \times 10^4$ $cm^{-1}$), the $(\Delta E - \hbar\omega)$ energy factor in the denominator does not vary much. The energy shift, $\Delta^2E$ increases with resonance effects. At the same time the $\Delta^2E_i^0$ factors decrease. The upshot is that a plot of $S_{yz}^2$ (i.e., intensity) vs. $\Delta^2E$ should yield a smooth monotonic curve. Such a plot is shown in Figure 5. The contrast between the OP and TP intensity–energy relationships for several substituted benzenes is clearly revealed in Figure 5, which shows the

(32) E. B. Wilson, Jr., *Phys., Rev.*, **45**, 706 (1934).
(33) J. H. Callomon, T. M. Dunn, and I. M. Mills, *Phil. Trans. R. Soc. London, Ser. A*, **259**, 499 (1966).
(34) R. Vasudev and J. C. D. Brand, *J. Mol. Spectrosc.* **75**, 288 (1979).
(35) K. Krogh-Jespersen, R. P. Rava, and L. Goodman, *Chem. Phys.*, **47**, 321 (1979).

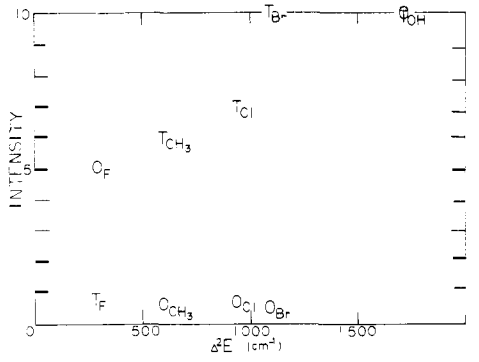


**Figure 5.** Plot of one- (O) and two- (T) photon intensity vs. shift in 0–0 band energy for several substituted benzenes relative to benzene showing the direct dependence of two-photon intensities on resonance interactions.

respective interference and lack of interference of the resonance and inductive effects in the two spectra.

Murrell's detailed calculations[21] of the wave functions and the spectra of aniline confirm the perturbation theory conclusion that the states become heavily scrambled. More than 16% and 45% of the $L_b$ and $B_b$ states are calculated to arise from $CT_b^0$ contamination. The CT terms are now so substantial that the TP $L_b$ spectrum may be best understood in terms of the strong coupling case. This means that the neglected square terms in eq 12 must now be included. The strong coupling extension of eq 13 becomes

$$S_{yz} = \left[\frac{2^{-1/2}}{\Delta E - \hbar\omega}\right][\langle A^0|\mu_y|B_b^0\rangle\{(\lambda(CT) - \Lambda(CT)) \times \langle\Phi_7|\mu_z|\Phi_3\rangle + \Lambda(CT)\lambda(CT)\mu_{CT}^0\}] \quad (14)$$

$\mu_{CT}^0$ represents the dipole moment of the molecules in the zeroth order CT state, and to a first approximation is $\mu_g - 2e\mathbf{R}$, assuming equal bond distances throughout the molecule.[36] ($\mu_g$ is the dipole moment of the ground state.) For aniline $\mu_g$ and $-2e\mathbf{R}$ ($\sim$12 D) have the opposite sense, thus $\mu_{CT}^0$ is substantially smaller than $\mu_g$. Nevertheless the estimated magnitude of $\mu_{CT}^0$ (-9 D (-3.5 au)) is large enough for the square term in eq (14) to provide an important correction if $\Lambda(CT)$ and $\lambda(CT)$ are large. Murrell's value of $\lambda(CT)\Lambda(CT)$ is $\sim -10^{-1}$. Thus this term is as major as the linear mechanism shown in Figure 2c, with the consequence that the TP intensity mechanism for aniline cannot be as simply visualized as for the intermediate coupling case. The intensity arises from the more complicated mechanism illustrated in Figure 2d, and the spectrum is expected to bear little resemblance to that exhibited by the intermediate coupling category molecules such as phenol.

Note should be taken of the possible contribution of doubly excited configurations to the TP intensity. In OP spectroscopy configurations of this type are normally neglected because two-electron electric dipole transition moments to the ground state vanish. In TP processes, however, the transition tensor involving contamination of $L_b^0$ (or $B_b^0$) by doubly excited configurations is formally allowed. Nevertheless perturbation theory calculations suggest that they provide unimportant contributions to the TP intensity.

## VIII. Concluding Remarks

We conclude that there is a direct correlation between the FC intensities in the TP spectra of substituted benzenes and the resonance interaction between the substituent and ring. This relationship is most clearly illustrated in Figure 5. No simple correlation of this sort is found for the OP intensities, where inductive effects interfere. A particularly lucid illustration of this difference in the two spectra is found for the halobenzenes (Figures 6 and 7). The OP FC intensity (Figure 6) correlates with the inductive effect (decreasing from F to Br), and the TP FC intensity (Figure 7) correlates with the resonance interaction (increasing from F to Br).

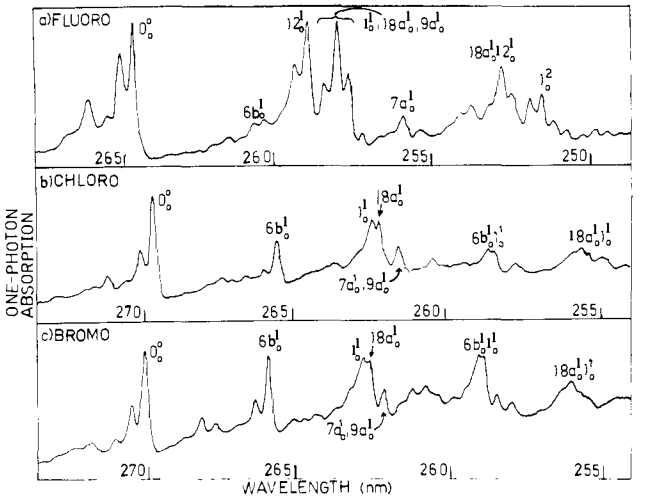


**Figure 6.** The fundamental region of the vapor one-photon absorption to the $^1L_b$ state of halobenzenes showing decrease of the FC intensity on going from fluorine to bromine and thus dependence of the spectra on the inductive effect.

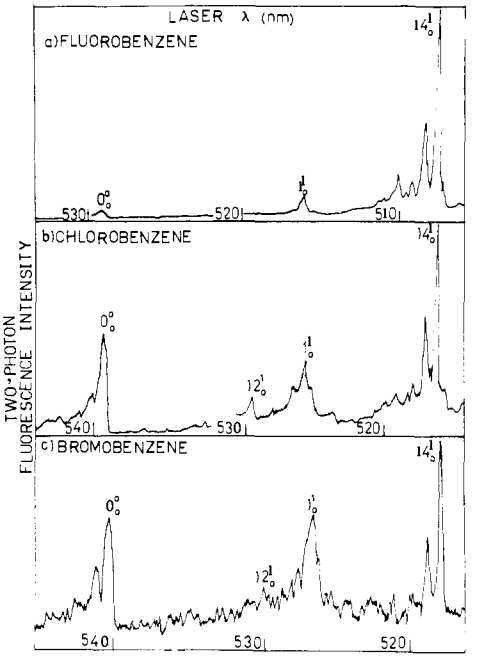


**Figure 7.** The fundamental region of the two-photon vapor fluorescence excitation spectra to the $^1L_b$ state of halobenzenes. The figure shows the growth of the FC intensity on going from fluorine to bromine and thus the spectra's insensitivity to the inductive effect.

The major thrust of this paper is that in revealing valence interactions TP spectra are not simply an extension of OP. We have focused on the B intermediate states to obtain concise conclusions. The full theory including the effect of other intermediate states and the extension to polysubstituted benzenes is given elsewhere.[38] New information can be gained which has not been feasible to obtain from OP spectroscopy. As further examples, we discuss in other publications how the TP spectrum of phenylacetylene provides an understanding of the valence interactions in this molecule[39] and how TP spectroscopy may be used to assess the importance of different valence bond structures to

(36) We estimate $\mu_{CT}^0$ by a point charge approximation involving transfer of an electron from $\Phi_7$ to the center of the benzene ring (i.e., a distance of $2R$). The observed value for $\mu_g$ is 2 D.[37]

(37) I. Fischer, *Nature (London)* **165**, 239 (1950).

(38) L. Goodman and R. P. Rava, "Advances in Chemical Physics", I. Prigogine and S. A. Rice, Eds., Wiley, New York, 1982.

(39) L. Chia and L. Goodman, *J. Chem. Phys.*, **76**, 4745 (1982).

chemical bonding involving elements in the thrid row. We have focused on only one such insight in this paper, the resonance ffect, but the fundamental ideas discussed here can be applied to illucidate concepts basic to chemical reactions.

**Acknowledgment.** Financial support from the National Science Foundation and the Rutgers Center for Computer and Information Studies is gratefully acknowledged. We thank Professor Karsten Krogh-Jespersen for helpful discussions, Dr. M. K. Haque for running the OP spectra and for checking the vibrational analysis of the phenol TP spectra, and Mr. Richard Cooke for obtaining preliminary phenol TP spectra. We express our appreciation to Professor Patrick Callis for sending a copy of his paper on pyrimidine prior to publication and for helpful correspondence.

**Registry No.** Benzene, 71-43-2; fluorobenzene, 462-06-6; phenol, 108-95-2; aniline, 62-53-3; chlorobenzene, 108-90-7; bromobenzene, 108-86-1; anisole, 100-66-3.

# Microwave Spectra and Molecular Structure of $BH(NH_2)_2$

**L. R. Thorne* and W. D. Gwinn**

*Contribution from the Department of Chemistry, University of California, Berkeley, California 94720.* *Received September 21, 1981*

**Abstract:** The effective molecular structure of boranediamine, $BH(NH_2)_2$, has been determined from the microwave spectra of eight isotopic species. The molecule has planar $C_{2v}$ symmetry, with $r$(B–H) = 1.193 ± 0.001 Å, $r$(B–N) = 1.418 ± 0.001 Å, $r(N–H_{cis})$ = 1.005 ± 0.005 Å, $r(N–H_{trans})$ = 1.000 ± 0.003 Å, ∠NBN = 122.0 ± 0.3°, $\angle BNH_{cis}$ = 121.1 ± 0.1°, and $\angle BNH_{trans}$ = 123.7 ± 0.6°, where the amine hydrogens are cis or trans relative to the boron-bonded hydrogen. The dipole moment is 1.245 ± 0.017 D.

The molecular structures of the boranamines have attracted interest since the first electronic structure calculations[1] developed for simple organic molecules were used to treat isoelectronic B–N-containing compounds. These and later calculations[2-6] showed that the B–N bonds of boranamines have partial double-bond character that results from delocalization of the nitrogen lone-pair electrons into the vacant boron $2p_z$ orbital. The degree of delocalization has important structural consequences. With no delocalization, the torsional barrier about the B–N bond is low, and the three nitrogen bonds assume a pyramidal configuration due to repulsion by the nitrogen lone pair. On the other hand, with sufficient delocalization, the three nitrogen bonds are coplanar, the torsional barrier is high, and the B–N bond length is shortened. In either situation, microwave spectroscopy permits determination of the molecular structure, the molecule's planarity, the height of the torsional barrier (if it is less than 5 kcal $mol^{-1}$) and the magnitude of the electric dipole moment.

Despite considerable theoretical interest, however, there has been a notable lack of experimental data on the structures of the unsubstituted boranamines, $BH_{3-n}(NH_2)_n$ ($n$ = 1, 2, or 3). This is due, in part, to the instability of condensed boranamine monomers,[7] which complicates their synthesis. Recently, however, boranediamine, $BH(NH_2)_2$, was isolated under normal conditions, and we reported its molecular structure based on preliminary microwave data.[8] Shortly thereafter, the microwave spectrum and partial structure of boranamine, $BH_2NH_2$, were reported by Suggie, Takeo, and Matsumura.[9] In the present paper we report the results of further investigation of the microwave spectrum of $BH(NH_2)_2$ and seven of its isotopic species. This study has yielded more accurate values for the rotational constants, molecular structure, and dipole moment than had been reported previously.

## Experimental Section

The microwave spectrometer used to measure the rotational spectra of boranediamine has been described in detail previously.[10,11] It employs Stark modulation at one of a number of selectable frequencies in the range 5–20 kHz. Both the microwave source and the data acquisition system are controlled by a laboratory minicomputer. The spectrometer has a large dynamic range and is capable of recovering weak signals by means of signal averaging and digital filtering of the data.

Reflex klystrons are used as microwave sources in the 8–40 and 44–48-GHz ranges. These sources are phase-locked to a 100-kHz, crystal-controlled secondary frequency standard by means of a harmonic multiplier and a series of phase-locked loops. Shottky diodes are used to detect the microwave signals in the 8–18-GHz region; point-contact diodes are used in all other frequency regions. The microwave cell is operated at −45 °C and 5–20-μm pressure, as monitored by a capacitance manometer.

Boranediamine was synthesized following a procedure developed by Briggs et al.,[8] in which a stream of dry ammonia is passed over molten borane ammoniate ($BH_3{\cdot}NH_3$). Obtaining high yields of boranediamine required excess ammonia, which was sublimed from the product at −104 °C. Samples free of detectable amounts of ammonia were difficult to prepare, both because the purification was not complete and because boranediamine decomposes to yield ammonia. The handling of boranediamine was complicated by its strong tendency to polymerize in the liquid phase and its high reactivity toward water. Gas samples below

* To whom correspondence should be addressed at the Noyes Laboratory of Chemical Physics, California Institute of Technology, Pasadena, CA 91125.

(1) Hoffman, R. *J. Chem. Phys.* **1964**, *40*, 2474–2480.
(2) Fjelberg, T.; Gunderson, G.; Jonvik, T.; Seip, H. M.; Saebo, S. *Acta Chem. Scand., Ser. A* **1980**, *34*, 547–565.
(3) Thorne, L. R. Ph.D. Thesis, University of California, Berkeley, CA, June 1979.
(4) Whiteside, R. A.; Frisch, M. J.; Binkley, J. S.; Defrees, D. J.; Schegel, H. B.; Raghavachari, K.; Pople, J. A. Carnegie-Mellon Quantum Chemical Archive, 2nd Ed; Department of Chemistry, Carnegie-Mellon University: Pittsburgh, PA, July 1981.
(5) Binkley, J. S., private communication. For further computational details see: Binkley, J. S.; Whiteside, R. A.; Kirshnan, R.; Seeger, R.; Defrees, D. J.; Shlegel, H. B.; Topiol, S.; Khan, L. R.; Pople, J. A. *QCPE* **1981**, *13*, 406.
(6) Dill, J. D.; Schleyer, P. v. R.; Pople, J. A. *J. Am. Chem. Soc.* **1975**, *97*, 3402–3409.
(7) Niedenzu, K.; Dawson, J. W. "Boron–Nitrogen Compounds"; Academic Press: New York, 1965; Vol. VI.
(8) Briggs, T. S.; Gwinn, W. D.; Jolly, W. L.; Thorne, L. R. *J. Am. Chem. Soc.* **1978**, *100*, 7762.
(9) Suggie, M.; Takeo, H.; Matsumura, C. *Chem. Phys. Lett.* **1979**, *64*, 573–575. Suggie, M.; Kawashima, K.; Takeo, H.; Matsumura, C. *Koen Yoshishu-Bunshi Kozo Sogo Toronkai* **1979**, 168–169.
(10) Renkes, G. D.; Thorne, L. R.; Gwinn, W. D. *Rev. Sci. Instrum.* **1978**, *49*, 994.
(11) Gwinn, W. D.; Luntz, A. C.; Sederholm, C. H.; Mullikan, R. *J. Comput. Phys.* **1968**, *2*, 439.

0002-7863/82/1504-3822$01.25/0 © 1982 American Chemical Society